Extensions of the Direct-Semidirect Model for Calculating the High Energy Component of Fast-Nucleon Induced Gamma Spectra

F. S. Dietrich

May 22, 2000

DISCLAIMER

EXTENSIONS OF THE DIRECT-SEMIDIRECT MODEL FOR CALCULATING THE HIGH ENERGY COMPONENT OF FAST-NUCLEON INDUCED GAMMA SPECTRA

FRANK S. DIETRICH

Lawrence Livermore National Laboratory

P. O. Box 808, Livermore, CA 94550, USA

ABSTRACT

This section reviews extensions and variations of the direct-semidirect (DSD) model for understanding the high-energy component of gamma spectra resulting from radiative capture of fast nucleons; i.e., the part of the spectrum that is not amenable to standard statistical model (Hauser-Feshbach) treatments. We describe recent results on the extension of the DSD model to unbound final states, including comparison with proton and neutron capture data. The importance of including convective-current magnetic radiation to explain proton capture angular distributions in the 30 MeV region is shown. We conclude with a brief discussion of a model closely related to the DSD, the pure-resonance model.

1. Introduction

In radiative capture of nucleons above a few MeV incident energy, the most energetic gammas are well understood as arising from direct reaction processes. Since its introduction 30 years ago, the direct-semidirect (DSD) model [1,2] has been the principal theoretical tool for interpreting this component of the gamma spectrum. In this model, direct radiative capture is supplemented by additional coherent amplitudes in which the incident nucleon excites giant resonances that subsequently decay by gamma emission. While both types of amplitudes are required for a full description of the capture process, semidirect excitation of the giant-dipole resonance (GDR) is dominant over a wide energy region about the position of the GDR. In addition to the dominant E1 multipolarity, higher multipolarities (M1, E2, E3) have also been included in DSD calculations.

Until recently, DSD calculations have been limited to capture to bound final states, and consequently only the portion of the gamma spectrum between the incident nucleon energy and the endpoint (approximately 8 MeV higher) has been available to this model. Consequently, the portion of the spectrum above the region where Hauser-Feshbach calculations apply (less than approximately 10-12 MeV) and below the region of bound final states has been calculated only with semiclassical pre-equilibrium models [3], or with multistep compound models that yield conflicting results [4,5]. A recent extension of the DSD model to unbound final states [6] that significantly expands the region of applicability of this model is reviewed in Section 2. This extended model is also applicable

to a portion of the bound final-state region where conventional DSD calculations are of limited usefulness because of fragmentation of the final single-particle orbitals among a dense background of complicated neighboring states.

Magnetic radiation of multipolarity higher than M1 has not previously been incorporated in DSD calculations. In Section 3 calculations are shown for the angular distributions of 34-MeV protons on medium and heavy nuclei that indicate the importance of convective current M2 and M3 radiation in the direct terms.

Difficulties in applying the DSD model to certain transitions in heavy nuclei (particularly neutron and proton capture on [208]Pb) led to the development of a closely related model, the pure-resonance model (PRM). This model [7,8], which is an approximation to DSD, was developed in the course of an examination of the consistency of the DSD model. A current view of this model and a recent application of it are presented in Section 4.

2. The Extended DSD Model for Capture to Unstable Final States

The direct-semidirect model has recently been extended to allow calculation of radiative capture to unstable final states [6]. Two types of unstable final states are included: 1) states in which the single-particle configuration following capture are unbound and may therefore decay into the continuum, and 2) single-particle states that are bound, but subsequently damp into the compound nucleus. In both cases, the correct treatment of the compound-nuclear damping is critical for the success of the model. The extended model was tested and shown to be successful by performing an experiment on radiative capture of 19.6-MeV polarized protons on [89]Y [6]. More recently, this model has been used to interpret 34-MeV proton-induced gamma spectra and angular distributions [9], as well as spectra from 14-MeV neutron capture [10].

The principal difference between the extended treatment and the standard DSD model is in the handling of the final state. In the standard DSD model, the final state of the captured particle is described by a bound-state wave function, usually obtained by solution of the Schrödinger equation for a Woods-Saxon well. In the extension of the model, all necessary information on the final state is determined by a complex (i.e., optical) potential, which is defined for both unbound and bound final-state single-particle configurations. For unbound final states, the imaginary potential describes damping of the simple single-particle state following capture into the compound nucleus. Similarly, for bound final states, the imaginary potential represents the spreading of the single-particle configuration into a dense spectrum of complicated states in the neighborhood of the final-state energy. The extended model reduces to the standard DSD calculation in the limit of vanishing final-state imaginary potential.

In the extended model for capture to unbound final-state configurations, the double-differential inclusive cross section (i.e., in which only the outgoing gamma is measured) is

$$\frac{d\sigma}{dE_\gamma d\Omega_\gamma} = \sigma_1 + \sigma_2 \, , \tag{1}$$

in which the first term on the right-hand side is

$$\sigma_1 = -\frac{1}{\phi_{inc}} \frac{2}{\hbar} \left(\frac{1}{\hbar c}\right)^3 E_\gamma^2 \left\langle \overline{\Psi}_i^{(+)} \left| H_\gamma G^{(+)\dagger} W G^{(+)} H_\gamma \right| \overline{\Psi}_i^{(+)} \right\rangle, \tag{2}$$

and the second is

$$\sigma_2 = \frac{1}{\phi_{inc}} \frac{2\pi}{\hbar} \left(\frac{1}{\hbar c}\right)^3 E_\gamma^2 \sum_p \left| \left\langle \tilde{\chi}_p^{(-)} \left| H_\gamma \right| \overline{\Psi}_i^{(+)} \right\rangle \right|^2 \delta(E - E_p). \tag{3}$$

For bound final-state configurations, the corresponding expression is

$$\frac{d\sigma}{dE_\gamma d\Omega_\gamma} = -\frac{1}{\phi_{inc}} \frac{2}{\hbar} \left(\frac{1}{\hbar c}\right)^3 E_\gamma^2 \, \text{Im} \left\langle \overline{\Psi}_i^{(+)} \left| H_\gamma G^{(+)} H_\gamma \right| \overline{\Psi}_i^{(+)} \right\rangle. \tag{4}$$

In these expressions, $\overline{\Psi}_i^{(+)}$ is the energy-averaged incident wave function at energy E_i; it is the optical-model wave function, plus resonant terms representing coupling to giant resonances that give rise to the semidirect amplitude. E_f and E_γ are the energies of the final nuclear state and gamma ray, respectively, while E is $E_i - E_\gamma$. H_γ is the electromagnetic operator. ϕ_{inc} is the flux of incident particles. $G^{(+)}$ is a Green's function (with appropriate boundary conditions) for the interaction of the captured nucleon with the target via a complex optical potential. W is the imaginary part of the optical potential, defined for both continuum and bound final states, and $\tilde{\chi}_p^{(-)}$ is an optical-model wave function for continuum final states. For the unbound case, Eq. (3) is the straightforward extension of the conventional DSD calculation. The additional term, Eq. (2), represents damping of the final-state configuration following capture, and in fact is the dominant term [6].

Calculations using the extended DSD model are shown in Figs. 1 and 2 and are compared to the results of the ^{89}Y(p,γ) experiment with 19.6-MeV polarized protons. Direct E1, E2, and E3 radiation as well as semidirect E1 were included.

Fig. 1 shows the measured 90° differential cross section, together with the extended DSD calculations and with Hauser-Feshbach calculations using the GNASH code [11] of the equilibrium statistical emission using two different prescriptions for the gamma-ray transmission coefficient [12,13]. The peak at 15.11 MeV is due to inelastic scattering on a carbon impurity in the target. The combination of DSD and Hauser-Feshbach calculations reproduces the data reasonably well, and additional multistep reaction mechanisms are not required. The DSD calculations were made with Eqs. (2) and (3) in the unbound region below 19.6 MeV gamma energy, and with Eq. (4) in the bound-state region above that energy. There is no discontinuity between these two regions. The DSD calculations were carried out to only 26 MeV, since the ground-state peak near 28 MeV is more appropriately treated by a conventional DSD calculation. The calculations show a transition between compound and direct processes in the region near 16 MeV.
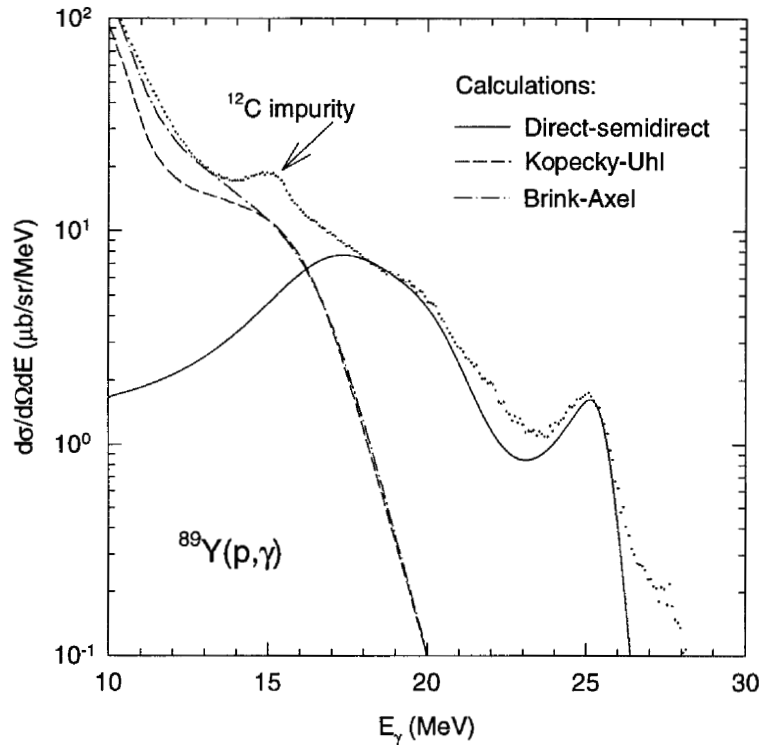
Figure 1. Unpolarized differential cross section at 90°. The data (dots) are shown together with the extended DSD model calculation (solid line), and with Hauser-Feshbach calculations using Kopecky-Uhl (dashed line) and Brink-Axel (dot-dashed line) gamma transmission coefficients. The calculations were folded with experimentally determined lineshapes before presentation with the data.

In Fig. 2 the extended DSD calculations are compared with the measured analyzing powers at the five angles for which data were taken. The data are well reproduced by the calculations, including the reversal in the sign of the asymmetries between the forward and backward hemispheres.

The calculations shown in Figs. 1 and 2 suggest that multistep contributions may not be important at energies up to approximately 20 MeV. To further investigate this issue, the model has been applied to gamma-production data [9] taken with 34 MeV protons on targets of Cu, Ag, and Au. Fig. 3 shows the spectrum at 75° for the Cu target. The parameters and calculational details were very similar to those in the $^{89}Y(p,\gamma)$ case with appropriate variations taking into account the incident and final state energies as well as the target Z and A.. However, the calculations have not been smeared with the experimental lineshapes, which should make little difference since the part of the spectrum of interest varies rather slowly with energy. The falloff in the spectrum below 10 MeV is due to an electronic cutoff. No further adjustment was made except for the final state well depth which was chosen to match known single-particle energies. In addition to direct E1,

E2, and E3 radiation as well as E1 semidirect, we have included convective-current direct M1 and M2. The importance of the magnetic radiation is shown in the next section.
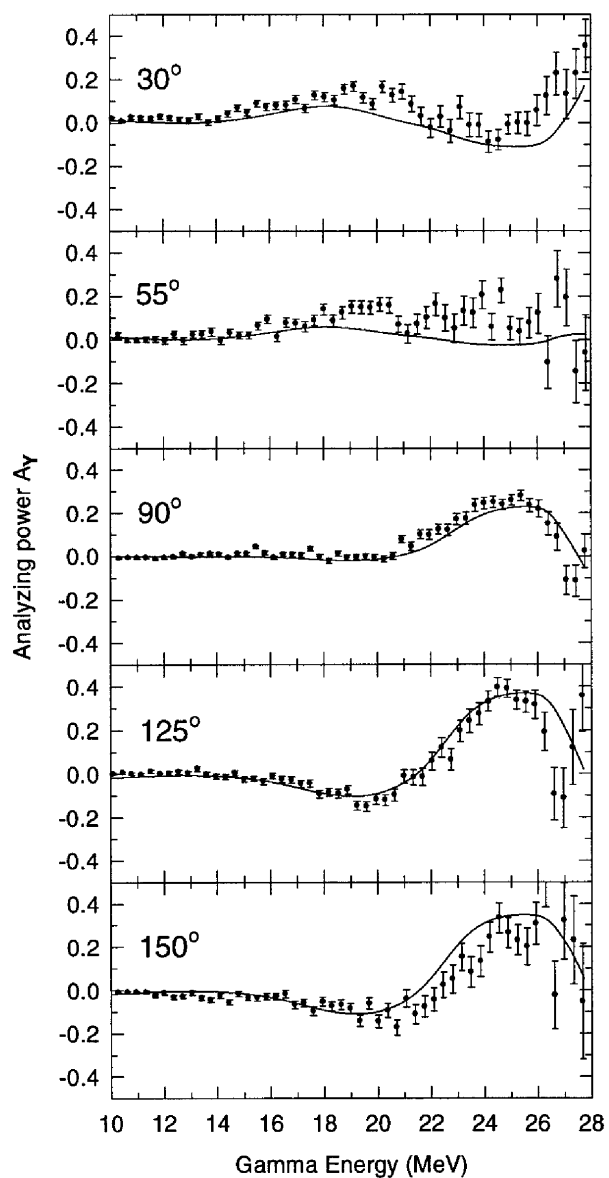

Figure 2. Measured analyzing powers compared with the extended DSD calculations. The calculations have been folded with the experimentally-determined lineshapes.
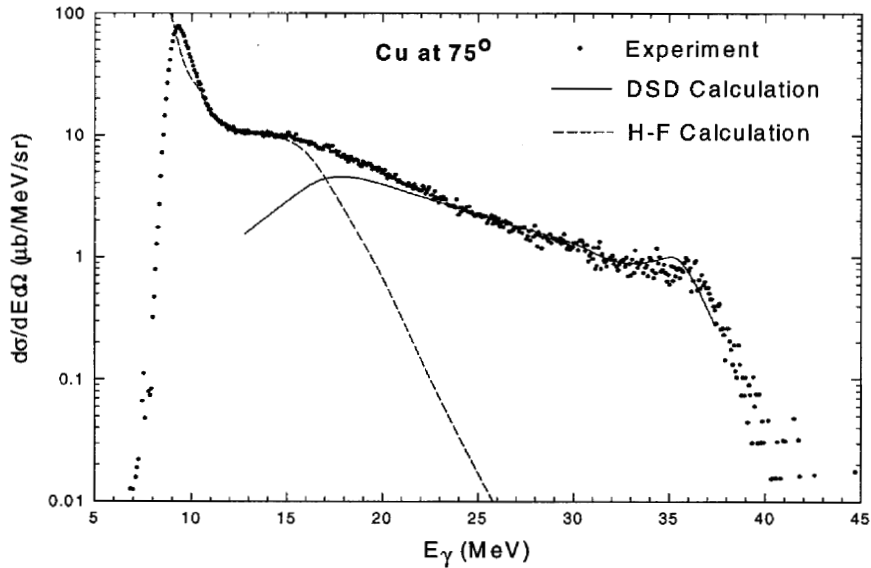
Figure 3. Spectrum of gammas at 75° from 34-MeV proton bombardment of Cu compared with extended DSD and Hauser-Feshbach calculations.

As was the case for ^{89}Y(p,γ) at 19.6 MeV, there is no apparent need for additional mechanisms to explain the spectrum. The results for Ag are of similar quality. The DSD calculation for Au lies below the data by about a factor of 2, which is likely due to the fact that no attempt was made to optimize the parameters for the higher mass region.

Additional tests have been performed for neutron capture near 14 MeV. The results for 14-MeV neutron capture on ^{89}Y, compared with the data of Budnar et al. [10], are shown in Fig. 4, together with a Hauser-Feshbach calculation. Parameters were similar to those for 19.6-MeV ^{89}Y(p,γ). The solid line is the DSD calculation, while the dashed line is the same calculation smeared by the experimental resolution. The combination of the smeared DSD and Hauser-Feshbach calculations is in excellent agreement with the experiment. In particular, the dip near 14 MeV gamma energy is reproduced. However, the experimental data of Rigaud et al. [14] are very different in magnitude and shape; there is neither a peak near 17 MeV nor a dip near 14 MeV. The disagreement between experimental data sets severely hampers tests of capture models at 14 MeV. These disagreements are discussed in Section B.3.2.2 of this report, together with an illustration of the differences between Refs. [10] and [14] for capture on ^{89}Y.

3. Effect of Higher Magnetic Multipolarities on Angular Distributions

Apart from occasional attempts to include M1 radiation, magnetic multipolarities have been ignored in DSD calculations. Although direct radiation higher than dipole of both magnetic and electric multipolarities is suppressed by effective charge factors for neutron
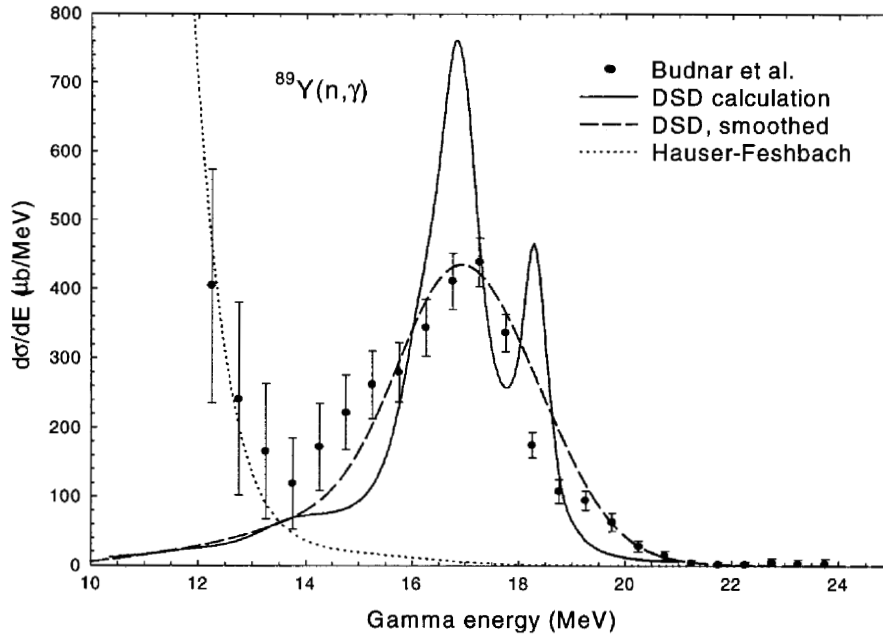
Figure 4. Comparison of extended DSD and Hauser-Feshbach calculations with the data of Ref. [10] for 14-MeV neutron capture on ^{89}Y. The calculations are shown both smeared by the experimental resolution and unsmeared. See text for a discussion of inconsistencies between experimental data sets for this reaction.

capture, this is not the case for capture of charged particles. Analysis of the 34-MeV proton capture data of Ref. [9] using the extended DSD model required investigation of this question. Convective current M1 through M4 direct capture amplitudes were incorporated in the code used to analyze these data. The spin current contributions were not included, since the convective currents are expected to be dominant because of the large orbital angular momenta (up to 8 or 10) required at these high energies.

Fig. 5 shows calculations that demonstrate the importance of the higher magnetic radiations on angular distributions in proton capture. The calculations are for 30.8 MeV gamma rays from capture on Au at 34 MeV proton energy. The curve labeled "E only" includes direct E1, E2, and E3 radiation as well as semidirect E1. The remaining curves show the effect of adding the magnetic radiations of orders M1 through M3. The calculations show that magnetic radiations are very important at forward and backward angles. While the magnetic radiations have a significant effect on the angular distributions, their effect on the angle-integrated cross sections is small. In the present case it appears that including M1 and M2 is sufficient. At still higher energies additional multipolarities, both electric and magnetic, should be required.

In Fig. 6 angular distributions calculated with the extended DSD model are compared with the 34-MeV proton capture data of Ref. [9]. Both calculations and experimental data have been integrated over a gamma-ray energy interval of 25 to 33 MeV.
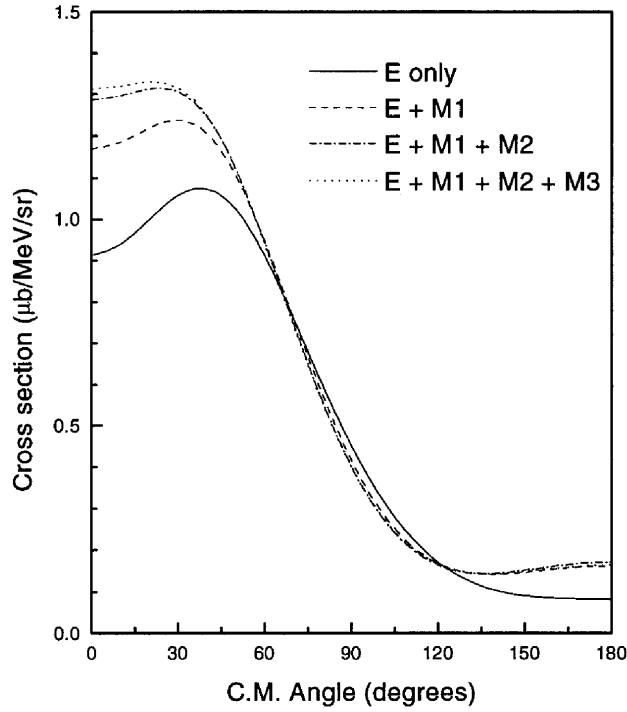
Figure 5. Angular distributions calculated with the extended DSD model for ^{197}Au(p,γ) at an incident energy of 34 MeV and a gamma energy of 30.8 MeV. The calculation labeled "E only" includes direct E1 through E3 and semidirect E1. The remaining curves show the effect of adding additional direct convective-current magnetic radiation.

4. The Pure-Resonance Model

The pure-resonance model (PRM) was developed to address questions of consistency between the two terms in the direct-semidirect model [7,8]. It was based on the two observations that 1) in the photoejection reaction (which is inverse to radiative capture) experimental data show symmetric resonant peaks without an obvious nonresonant contribution; and that 2) the direct amplitude in DSD contains a giant-resonance contribution, since the incident optical-model wave function is not orthogonal to the giant resonance.

The PRM results from reformulating the capture model so that the continuum wave function appearing in its matrix elements no longer contains giant-resonance components. This is accomplished by using projection operator techniques as developed for the photonuclear problem by Wang and Shakin [15]. Using these techniques, the direct-semidirect amplitude

$$c_1 + \frac{c_2}{E_\gamma - E_{GDR} + \frac{1}{2}i\Gamma_{GDR}} \tag{5}$$

may be formally rearranged (neglecting an unimportant small term) as

$$\frac{c_3 - c_4}{E_\gamma - E_{SP} + \frac{1}{2}i\Gamma_{SP}} + \frac{c_5}{E_\gamma - E_{GDR} + \frac{1}{2}i\Gamma_{GDR}}$$

(6) in which c_1 through c_5 are matrix elements calculated with ordinary optical wave functions in the DSD case (Eq. (5)), or projected wave functions for the PRM (Eq. (6)). E_{SP} and Γ_{SP} are the position and width of a single-particle resonance in the entrance channel, and are computed from the optical potential. The single particle resonance lies in the region of approximately 8 to 10 MeV. E_{GDR} and Γ_{GDR} are the position and width of the giant dipole resonance.
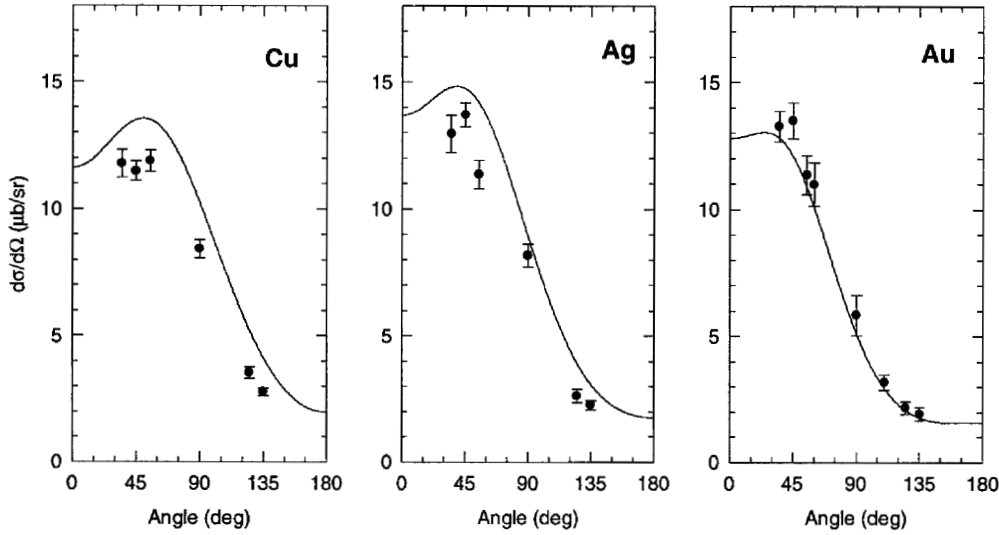

Figure 6. Extended DSD calculations and experimental data for angular distributions of 25 to 33 MeV gammas from 34-MeV proton capture on Cu, Ag, and Au.

In Eq. (6), c_3 and c_4 are both large and nearly cancel. Thus, a potential instability that is implicit in the DSD model is exhibited explicitly in the PRM formulation. In the pure-resonance model this instability is eliminated by assuming that this cancellation is exact, leaving only the giant resonance term.

A recent experiment [16] on the ^{40}Ca(n,γ_0) reaction, which was performed to search for the isovector quadrupole giant resonance, shows the usefulness of the PRM. Fig. 7 shows the data for this reaction, together with two calculations that included E1 and E2 radiation. The right-hand panel shows the 90° differential cross section, while the left-hand shows the fore-aft asymmetry A(55°), defined as $[\sigma(55°) - \sigma(125°)]/[\sigma(55°) + \sigma(125°)]$, where σ is the differential cross section. The solid curves used DSD for both E1 and E2, whereas the dashed curves were calculated using PRM for E1 and DSD for E2.

In the case shown in Fig. 7, it is apparent that the PRM yields a better reproduction of the experiment than the DSD. However, it should be noted that the approximation of neglecting the first term in Eq. (6) may be extreme, and that this approximation may not

be necessary if the consistency between the direct and semidirect terms in the DSD model is better understood than at present. Further work should be done in this direction.
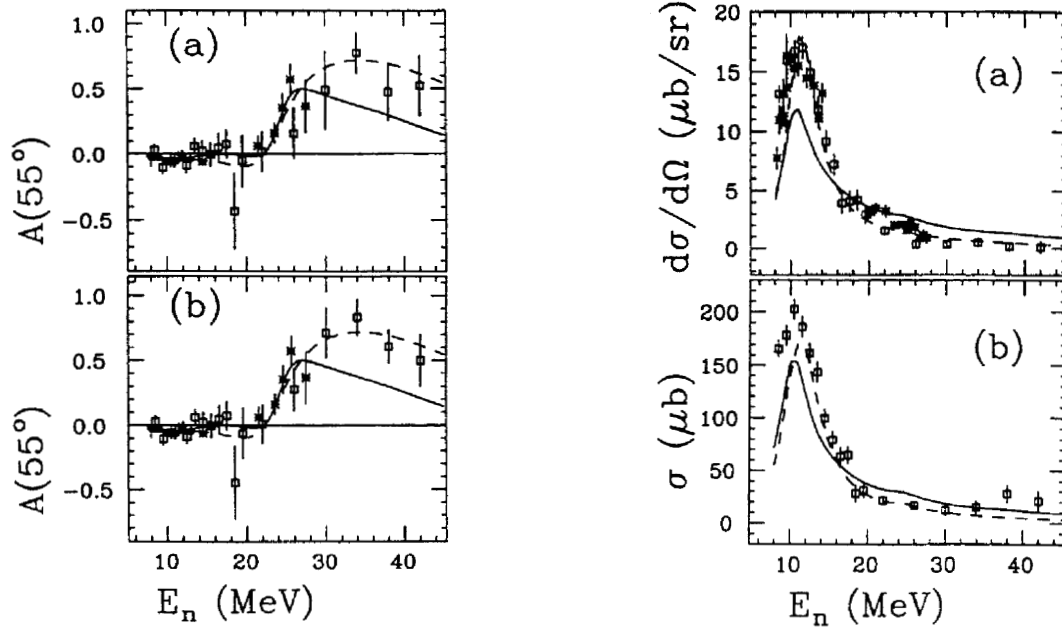

Figure 7. Fore-aft asymmetry (left panel) and 90° differential cross section (right panel) in the ^{40}Ca(n,γ_0) reaction [16]. Calculations were made with DSD for E1 and E2 amplitudes (solid curves), and with PRM for E1 and DSD for E2 (dashed curves).

5. Acknowledgments

6. References

1. G. E. Brown, Nucl. Phys. **57**, 339 (1964).
2. C. F. Clement, A. M. Lane, and J. R. Rook, Nucl. Phys. **66**, 273,293 (1965).
3. E. Betak, contributions to this report and references therein.
4. P. Oblozinsky and M. Chadwick, Phys. Rev. **C42**, 1652 (1990).
5. M. Herman, A. Höring, and G. Reffo, Phys. Rev. **C46**, 2493 (1992).
6. W. E. Parker *et al.*, Phys. Rev. **C52**, 252 (1995).

7. F. S. Dietrich and A. K. Kerman, Phys. Rev. Lett. **43**, 114 (1979).

8. F. S. Dietrich, in AIP Conference Proceedings No. 125, Capture Gamma-Ray Spectroscopy, Knoxville, TN, 1984, p. 445.

9 S. J. Luke, Ph.D. thesis, University of Washington, 1992 (unpublished).

10. M. Budnar *et al.*, IAEA report INDC(YUG)-6 (1979).

11. P. G. Young, E. D. Arthur, and M. B. Chadwick, Los Alamos National Laboratory Report LA-12343-MS (1992).

12. D. M. Brink, Ph. D. thesis, Oxford University (1955); P. Axel, Phys. Rev. **126**, 671 (1962).

13. J. Kopecky and M. Uhl, Phys. Rev. **C41**, 1941 (1990).

14. F. Rigaud *et al.*, Nucl. Phys. **A154**, 243 (1970).

15. W. L. Wang and C. M. Shakin, Phys. Rev. **C5**, 1898 (1972).

16. C. M. Laymon, R. O. Nelson, S. A. Wender, and L. R. Nilsson, Phys. Rev. **C46**, 1880 (1992).